JACS
JOURNAL OF THE AMERICAN CHEMICAL SOCIETY

Article

pubs.acs.org/JACS

Phosphate–Water Interplay Tunes Amorphous Calcium Carbonate Metastability: Spontaneous Phase Separation and Crystallization vs Stabilization Viewed by Solid State NMR

Shifi Kababya,[†] Assaf Gal,*[,§] Keren Kahil,[‡] Steve Weiner,[‡] Lia Addadi,[‡] and Asher Schmidt*[,†]

[†]Schulich Faculty of Chemistry and Russell Berrie Nanotechnology Institute, Technion—Israel Institute of Technology, Haifa 32000, Israel

[‡]Department of Structural Biology, Weizmann Institute of Science, Rehovot 76100, Israel

Supporting Information

ABSTRACT: Organisms tune the metastability of amorphous calcium carbonates (ACC), often by incorporation of additives such as phosphate ions and water molecules, to serve diverse functions, such as modulating the availability of calcium reserves or constructing complex skeletal scaffolds. Although the effect of additive distribution on ACC was noted for several biogenic and synthetic systems, the molecular mechanisms by which additives govern ACC stability are not well understood. By precipitating ACC in the presence of different PO_4^{3-} concentrations and regulating the initial water content, we identify conditions yielding either kinetically locked or spontaneously transforming coprecipitates. Solid state NMR, supported by FTIR, XRD, and electron microscopy, define the interactions of phosphate and water within the initial amorphous matrix, showing that initially the coprecipitates are homogeneous molecular dispersions of structural water and phosphate in ACC, and a small fraction of P-rich phases. Monitoring the transformations of the homogeneous phase shows that PO_4^{3-} and waters are extracted first, and they phase separate, leading to solid–solid transformation of ACC to calcite; small part of ACC forms vaterite that subsequently converts to calcite. The simultaneous water–PO_4^{3-} extraction is the key for the subsequent water-mediated accumulation and crystallization of hydroxyapatite (HAp) and carbonated hydroxyapatite. The thermodynamic driving force for the transformations is calcite crystallization, yet it is gated by specific combinations of water–phosphate levels in the initial amorphous coprecipitates. The molecular details of the spontaneously transforming ACC and of the stabilized ACC modulated by phosphate and water at ambient conditions, provide insight into biogenic and biomimetic pathways.

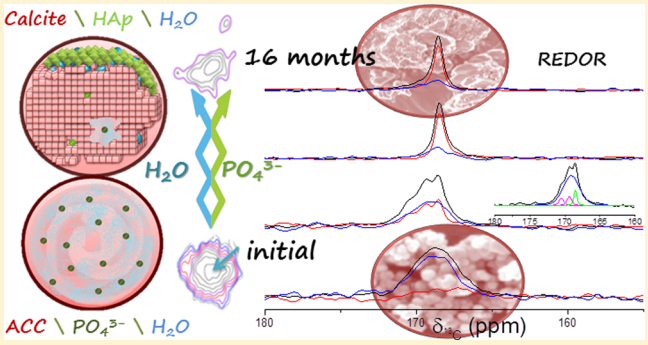

INTRODUCTION

Crystalline calcium carbonate in the form of aragonite and calcite is probably the most widespread mineral formed by organisms.[1−4] Many organisms first produce a highly disordered form of calcium carbonate, called amorphous calcium carbonate (ACC), which then crystallizes into either aragonite or calcite.[5,6] The ACC is often produced intracellularly in vesicles and is then exocytosed into the extracellular environment, where it crystallizes under controlled conditions.[7−10] Other organisms produce ACC that is stable at least during the lifetime of the organism or of the tissue in which the ACC is located.[3] These were identified as two classes—"transient" and "stable" ACC.

ACC can be produced in vitro by the rapid mixing of concentrated solutions containing calcium and carbonate.[11] Crystallization ensues almost immediately if the ACC is left in solution, whereas if dried immediately after precipitation, then ACC remains stable over time.[12] The transformation process can be better controlled by adding various ions, such as phosphate, silicate, or magnesium.[13−17] These additives both poison the formation of nascent nuclei in the solution, thus allowing high levels of supersaturation to be achieved, and after the formation of ACC, they also reduce the chance of a nucleus forming.[18] The latter occurs because phosphate and silicate, and to some extent Mg with its tightly coordinated water molecules, are bulky ions that when present above threshold levels, disrupt the lattice of any crystalline form of the planar carbonates, a phenomenon referred to as "geometric frustration".[19] It has been shown that certain proteins extracted from mineralized tissues as well as high and low molecular weight additives and metabolites can also induce the formation of ACC and stabilize it in vitro over time.[20−23]

A characteristic feature of biogenic ACC, such as in plant cystoliths,[24] crustacean cuticles[15] and gastroliths,[25] and in many highly disordered phases, including silica and amorphous

Received: November 25, 2014
Published: December 19, 2014

DOI: 10.1021/ja511869g
J. Am. Chem. Soc. 2015, 137, 990−998

calcium phosphate,[26] is that they are composed of nanospheres about 20−40 nm in diameter.[27,28] In fact, many mature crystalline biogenic phases, such as calcitic sponge spicules,[29] coral skeletons,[30] sea urchin spines[31] and larval spicules,[32] mollusk shells, and brachiopod shells,[33] all have a nanosphere texture even though they are crystalline. These observations led to suggest that the crystalline particles formed via an ACC precursor phase.[6]

Analyses of mineralized tissues composed of stable biogenic ACC reveal that a common additive used by a variety of organisms is phosphate. In crustacean gastroliths, inorganic phosphate was found to be molecularly dispersed throughout the ACC as a solid solution.[22] In lobster cuticle, ACC was shown to progressively transform upon heating into a mixture of segregated calcite and carbonated apatite crystalline phases.[34,35]

It has also been demonstrated that water is an integral component of stable ACC and is present in the proportions of approximately one mole of water for one mole of calcium carbonate in stable biogenic ACC.[36] Transient biogenic ACC from the well-studied sea urchin larval spicule appears to undergo several stages of transformation before becoming mostly calcite,[32,37] still retaining some residual ACC. These stages are assumed to involve progressive dehydration.

In a recent in vitro study of the transformation process of ACC into calcite, Gal et al. showed that if phosphate is present in the aqueous ACC, then the transformation process appears to involve two mechanisms: translocation of ACC nanospheres to the surface of the forming crystal where they crystallize, and dissolution of some of the ACC followed by ion-by-ion crystal growth.[24] The end product is a crystal having a texture composed of nanospheres and also expressing crystal faces. Much still remains to be understood about the mechanism of ACC transformation into crystalline polymorphs,[38] and what mechanisms prevent its transformation. What is the distribution of the additives in the initial ACC precipitates, what is the fate of the additives during transformation to the crystalline products, and does the structural water that is released from the ACC actually form localized concentrations of liquid water? These open questions are addressed in this study.

Recently, solid state NMR techniques that rely on dipolar interactions were shown to be invaluable in characterizing minute interaction regions in intact calcium carbonate biominerals. These include the buried and exposed interfaces in the aragonitic mollusk shell of *Perna canaliculus*,[39] and the directed incorporation of intracrystalline structural defects of phosphate and nitrate within the calcitic coccoliths of *Emiliania huxleyi*, *Gephyrocapsa oceanica*, and *Pleurochrysis carterae*.[40] Within gastrolith ACC the molecular dispersions of phosphate and two primary metabolites (phosphoenolpyruvate and citrate) were identified as the factors responsible for its stability.[22] Herein we extend the use of solid state NMR (^{13}C, ^{31}P, ^{1}H) as the main tool to monitor in vitro the ambient *spontaneous* phase separation and crystallization into calcite and carbonated hydroxyapatite of hydrated synthetic ACC metastabilized by phosphate. Also, conditions which lead to stable, locked ACC are identified and characterized. These observations shed light on the biomineralization pathways that involve ACC transforming into crystalline products, as well as the stabilization of ACC during the lifetime of some organisms.

RESULTS

General Characterization of the Initial Precipitates. Synthetic ACC samples were precipitated by rapid mixing of calcium and carbonate solutions, to yield supersaturated calcium carbonate solutions that were rapidly dried after precipitation, to prevent crystallization. The phosphate concentrations in the calcium carbonate solutions before precipitation were 0, 6, and 18 mM phosphate. The respective precipitates are denoted P-free-ACC, low-P-ACC, and high-P-ACC. Elemental analyses show that the precipitates contain 0, 6, and 17 mol % P/Ca (Supporting Information (SI) Table S1). The amorphous precipitates are composed of ∼20 nm spherical particles, characterized by scanning electron microscopy (SEM), transmission electron microscopy (TEM), and electron diffraction (SI Figure S1). Infrared absorption spectra have the characteristic carbonate vibrations of ACC and the phosphate vibrations of amorphous calcium phosphate (ACP; in the P-containing samples), and show no evidence of a crystalline phase (SI Figure S2). Heating of these precipitates followed by FTIR analysis shows that the P-free-ACC transforms into calcite after heating to 300 °C, the low-P-ACC transforms into calcite after heating to 350 °C, and the high-P-ACC transforms only after heating to 400 °C (SI Figure S2). Phosphate therefore stabilizes ACC, and higher phosphate concentrations stabilize it to a greater extent. The transformation of pure ACP into carbonated hydroxyapatite (cHAp) occurs only after heating to 500 °C; higher than any of the transformation temperatures of phosphate-stabilized ACC.

Two initial hydration levels of the coprecipitates were examined: (*i*) hydrated, as-prepared after 30 min under an IR lamp; (*ii*) dehydrated, after 2 days at 50 °C. The water content for the hydrated and dehydrated samples in the high- and low-P-ACC, derived from TGA (SI Figure S3), are summarized in SI Table S1. Accordingly, (*i*) and (*ii*) will be used to denote the two initial hydration states of the precipitates. We also prepared as a reference a finely ground physical mixture of P-free-ACC with ACP at a P/Ca molar proportion similar to the high-P-ACC (40 mg ACC, 7 mg of ACP).

Solid State NMR Characterization of the Initial Precipitates. The precipitates were subjected to solid state NMR characterization and contrasted with those of the P-free ACC and ACP, and of the ACC/ACP physical mixture. ^{13}C and ^{31}P MAS NMR spectra of all initial coprecipitates (high-P-ACC: Figure 1a, bottom-left projections, and SI Figure S4, low-P-ACC) exhibit the characteristic ACC and ACP spectra ($\delta[\delta\nu]$: ∼168.8[3.5], ∼3.8[5.2] ppm); their peak positions and widths are insensitive to the level of phosphate content. Notably, the ^{13}C MAS spectra, whether acquired by direct excitation (DE) or by cross-polarization (CP) are indistinguishable. Likewise, the ^{31}P DE- and CP-MAS spectra are also indistinguishable. Since only the hydrogen atoms of water molecules are the source of the carbonate and phosphate peaks in the respective CP-MAS spectra, the similarity of the CP and DE spectra demonstrates that water molecules are uniformly dispersed throughout the coprecipitates. The $\{^{1}H\}^{31}P \rightarrow {}^{13}C$ 2D-TEDOR NMR spectra (Figure 1a) of all initial precipitates show a single, broad $\{^{31}P,^{13}C\}$ crosspeak {3.8,168.8 ppm}, indicating that phosphates are molecularly dispersed throughout the ACC. Similar to the 1D spectra, also the crosspeaks of the 2D-TEDOR spectra are insensitive to the PO_4^{3-} abundance in the coprecipitates, and report the same structural/chemical environments (Figure 1a and SI Figure S5a).

DOI: 10.1021/ja511869g
J. Am. Chem. Soc. 2015, 137, 990−998

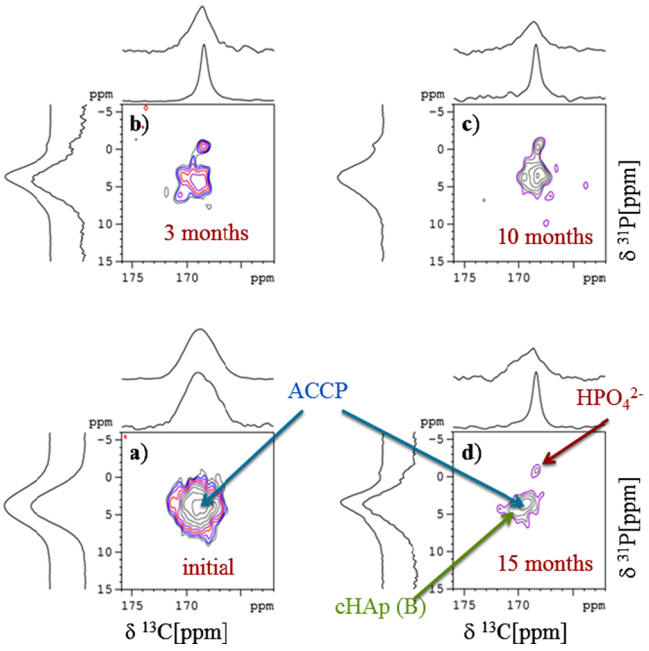

Figure 1. $\{^1H\}^{31}P \rightarrow {}^{13}C$ 2D TEDOR spectra of the high P-ACC(*i*) precipitate as a function of time. The initial spectrum (a) shows one broad crosspeak that represents homogeneous dispersion of phosphates and water in ACC, named ACCP. The intermediate spectra (b and c) show the breakdown path of the initial broad crosspeak. At the final stage (d), well resolved crosspeaks are observed for residual stabilized ACCP and HPO_4^{2-}. The latter is attributed to intracrystalline structural defects entrapped in calcite upon phase separation and crystallization. Notable is also the partially resolved crosspeak due to carbonates entrapped in HAp, representing B-type cHAp. The chemical shifts are listed in Table 1. The 1D-spectra are the DE- and CP-MAS spectra (next and remote from the axis, respectively).

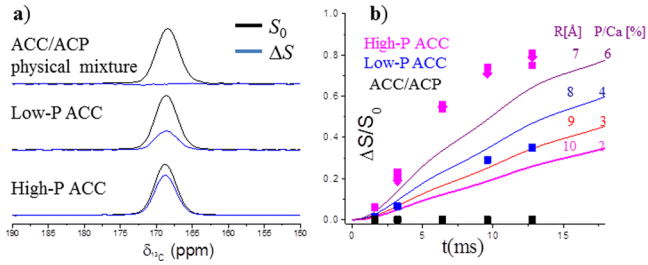

Figure 2. (a) $^{13}C\{^{31}P\}$ CP-REDOR MAS NMR spectra of the initial coprecipitates—high-P-ACC(*i*) (bottom), low-P-ACC(*ii*) (middle), and the ACC/ACP physical mixture; reference spectrum, S_0, black and difference spectrum, ΔS, blue, are overlaid. While the S_0 spectrum accounts for all carbon species, the difference spectrum ΔS (blue) shows peaks only for species that are nearby a P atom. The recoupling period is $64T_R$ (12.8 ms). (b) $^{13}C\{^{31}P\}$ CP/DE-REDOR MAS $\Delta S/S_0$ evolution. Experimental data points are shown for the initial high-P-ACC(*i*), (*ii*) coprecipitates (pink; 3 independent batches) and low-P-ACC(*ii*) (blue) and of the ACC/ACP physical mixture (black). The curves are REDOR simulations (SpinEvolution)[41] for a simplified geometric model of a phosphate centered in a $CaCO_3$ sphere with radii R = 7, 8, 9, 10 Å. The simulation assumes contributions from single $^{13}C\cdots^{31}P$ pairs with distances between 3 Å to R, weighted according to the fractional volume of the spherical shell (1 Å thickness) relative to the sphere volume (Table S3 in ref 22).

The dispersions of phosphates in the low- and high-P coprecipitates are clearly distinguished by $^{13}C\{^{31}P\}$ CP-REDOR NMR measurements.[42,43] Qualitatively, the increasing relative intensity of the REDOR difference peak, $\Delta S/S_0$, from the low-P-ACC to high-P-ACC coprecipitates, indicates an increasing percentage of carbonates which are up to 9 Å from a phosphate moiety (Figure 2a). The absence of a $^{13}C\{^{31}P\}$ CP-REDOR effect for the physical mixture of ACC/ACP shows the scarceness of molecular contacts, in contrast to their high abundance in the coprecipitates. A quantitative assessment of phosphate dispersion in ACC is obtained when measuring and analyzing the REDOR dipolar evolution curves of the coprecipitates (Figure 2b). Low-P-ACC exhibits a REDOR evolution, which is consistent with a simulated curve representing a homogeneous dispersion of PO_4^{3-} within ACC, such that on the average a phosphate is present within each sphere of 9 Å radius.[22] This translates into ~3 mol % P/Ca, whereas the elemental analysis shows the presence of 5.6 mol % P/Ca (SI Table S1). High-P-ACC exhibits much steeper REDOR evolution that reflects the much higher concentration of dispersed phosphate, in excess of 7 mol % P/Ca; the elemental analysis shows 17 mol % P/Ca. As the REDOR evolution is steeper than that represented by the 7 Å sphere, multiple phosphates occur at unknown geometries and REDOR cannot be used to provide a quantitative estimate. In conclusion, the above data identify the initial coprecipitates as amorphous calcium carbonates where water and PO_4^{3-} are molecularly and homogeneously dispersed. We denote these homogeneous phases as ACCP. The concentration of dispersed phosphate is much higher in the high-P-ACC. Since the P content reported by ICP is higher than that reported by the REDOR, the occurrence of separate ACP phases cannot be ruled out (to a larger extent in the high-P-ACC vs the low-P-ACC); distinguishing and quantifying the co-occurrence of ACCP and ACP is not possible given their similar spectroscopic NMR characteristics.

Spontaneous Phase Separation and Amorphous-to-Crystalline Transformation. We monitored the states of the ACCP materials as a function of time for up to 20 months using solid state NMR. A spontaneous phase separation followed by crystallization was observed to occur with time. Herein we describe in detail the NMR characterizations of the transformation of the hydrated high-P-ACC with time, while the respective data of the low-P-ACC that were monitored with coarser time intervals is described briefly at the end of the Results and in more detail in the SI. The transforming low-P-ACC coprecipitates yielded the same final components as the high-P-ACC.

The ^{13}C DE MAS spectra (Figure 3, black traces) clearly show that a spontaneous amorphous-to-calcite phase transformation takes place over time, which in part progresses via a vaterite intermediate (Figure 3b, 2 weeks). The vaterite is unambiguously characterized and is only present in the 2 week old sample. The transformation from ACC to the crystalline polymorphs involves extraction of water and phosphate from the calcium carbonate matrix (vide infra). Hydrogen atom scarcity upon removal of water precludes cross-polarization to *all* carbonates, however direct excitation quantitatively represents the various components in the system, and abundances can be estimated from deconvolution of the peaks (SI Figure S6). Cross-polarization emphasizes the remaining hydrated/hydrogenated environments and enables their detailed identification and characterization by deconvolution of the combined spectral evidence (1D and 2D; DE and CP) in a self-consistent manner. The results for the initial and

DOI: 10.1021/ja511869g
J. Am. Chem. Soc. 2015, 137, 990−998

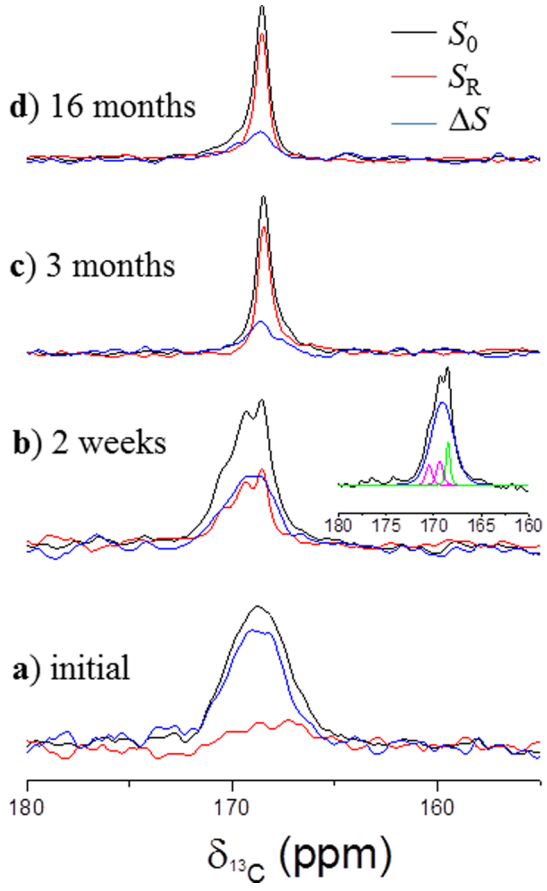

Figure 3. $^{13}C\{^{31}P\}$ DE-REDOR MAS NMR spectra ($64T_R$; 12.8 ms) of high-P ACC(*i*) as a function of time from preparation to 16 months. For every time point the reference spectrum, S_0 (black), REDOR spectrum S_R (red), and difference spectrum ΔS (blue) are overlaid. While the S_0 spectrum accounts for all carbon species, the difference spectrum ΔS shows peaks only for species that are within 9 Å from a P atom. The inset shows a representative deconvolution of the reference spectrum (S_0) obtained for high-P ACC after 2 weeks, showing the three carbonate species of calcite (green), vaterite (pink) and ACCP (blue). The spectra were acquired using a 2400 s repetition time to enable quantitative peak deconvolution. The resulting relative intensities for the three REDOR spectra at each time point are listed in SI Table S2.

final (16 months) coprecipitates are listed in Table 1. After 2 weeks 23% and 20% of the carbonates are calcitic and vateritic, respectively. After three months calcite reaches its final level of just over 72% of the carbonates, while only residual vaterite content remains (<1%). The ACCP content gradually decreases to about half (45%) after 2 weeks and to a fifth (20%) after three months or longer. Throughout the spontaneous process, two additional carbonate species evolve. The first, at 170.6 ppm, is identified as a type B carbonated-hydroxyapatite (cHAp-B; PO_4^{3-} substitution by CO_3^{2-}, vide infra),[45,46] reaching ~5% after one year. The second, a broad peak centered at 167.4 ppm, is of unknown chemical identity and is inferred to represent a collection of low abundance unresolved species (vide infra).

In addition to following the crystallization process, the actual progression of the phase separation is clearly documented by the $^{13}C\{^{31}P\}$ DE-REDOR spectra (Figure 3; S_R red, ΔS blue). As time elapses, the relative intensity of the carbonate difference peak decreases (ΔS), indicating that the fraction of

Table 1. Chemical Shifts, $\delta(^{13}C)$, $\delta(^{31}P)$, $\delta(^{1}H)$, and Representative Line Widths ($\delta\nu$) of the Different Species in the Initial and Final (16 Months) High-P and Low-P Coprecipitates, and the Relative Abundances of the Carbonate Species[a]

	$\delta^{13}C$ ($\delta\nu$) [ppm]	$\delta^{31}P$ ($\delta\nu$) [ppm]	$\delta^{1}H$ ($\delta\nu$) [ppm]	% C High-P	% C Low-P
start					
ACCP	168.8 (3.5)	3.8(5)	5.0	100	100
final (16 months)					
ACCP	169.2 (1.7)	3.9 (5)	5.5	23	9
Calcite	168.5 (0.7)			72	79
Vaterite	169.4 (0.7) 170.5 (0.7)			< 1	<1
HAp		3.3 (2.4)	-0.2	-	-
cHAp	170.6 (2.0)	4.5	-0.8	5	2
HPO_4^{2-}		-0.6 (1)	13	-	-
unknown	167.4 (2.7)		9	<1	11
HCO_3^-	168.5 (0.8)		14.3	<1	

[a]% C reflects mol % abundance of a species relative to the entire carbon content. The abundances are obtained from deconvolution of the ^{13}C DE MAS spectra which is assisted by the chemical shift information from the CP MAS (1D and 2D) spectra; scatter is ±5% for species with abundances above 30%, and ±50% for species with abundances below 15%. For species detectable only in the CP spectra (1D or 2D), but not in the 1D DE spectra, a value of <1% is listed as a default. To correct for the partial relaxation of calcite and vaterite in the DE spectra ($T_1 \approx 40$ min) their integrated peak intensities were multiplied by 1.6(44). "start" refers to all initial precipitates; "final" refers to high-P-ACC(*i*) and low-P-ACC(*ii*).

carbonates that is proximate to phosphate anions (<9 Å) becomes smaller. This clearly shows that the system components reorganize, namely, ions migrate from within the crystallizing calcium carbonates, enabling the buildup of the crystalline lattices. Already after 2 weeks, the REDOR spectra report that phosphates were removed from the vicinity of most crystalline carbonates, calcite and vaterite (Figure 3b–d, SI Figure S6 and Table S2). Interestingly, the calcitic component, once formed, shows a small extent of contacts with phosphates, $\Delta S/S_0 \leq 16\%$ (SI Table S2), yet no such contacts are detectable for the vaterite. This observation indicates that P-containing calcite did not develop from vaterite and attests for the coexistence of two parallel pathways of calcite formation. Most of the calcitic contacts are with HPO_4^{2-} species, which are entrapped as structural defects during the incomplete phase separation. This assignment is substantiated by both the well resolved −0.6 ppm peak in the 1D ^{31}P spectra of the aged precipitates, and by the 2D-TEDOR crosspeak {−0.6,168.5 ppm} showing HPO_4^{2-} connectivity to calcite carbonates (Figure 1b–d for high-P-ACC and SI Figure S5b,d for low-P-ACC).[47,48]

For the remaining ACCP and for the cHAp, carbonate contacts with P persist, as shown by their intense difference peaks in the CP-REDOR spectra (SI Table S2; $\Delta S/S_0 \geq 65\%$). In particular for ACCP, the relative REDOR difference peaks grow larger compared to those of the initial ACCP (SI Table S2). Moreover, the chemical shift deviates slightly and the peaks narrow slightly (SI Figure S6, Table 1) relative to those of the initial ACCP. These observations, taken together, indicate that the initial amorphous phase also undergoes rearrangement, becoming progressively more ordered. This phase has higher structural uniformity with tighter carbonate-phosphate contacts and/or increased abundance of its P-content. We note that the REDOR contacts detected for cHAp

DOI: 10.1021/ja511869g
J. Am. Chem. Soc. 2015, 137, 990–998

represent carbonates embedded in a P-rich matrix, while the detectable contacts in ACCP and of the HPO_4^{2-} defects in calcite represent phosphates dispersed in a "sea" of carbonates. Molecular contacts with P are also implied for the unidentified heterogeneous 167.4 ppm species.

To elucidate how the water molecules evolve during the process of crystallization and phase separation, we first examine their ^{1}H MAS NMR spectra. The initial coprecipitates show a broad water peak (Figure 4) which significantly narrows and

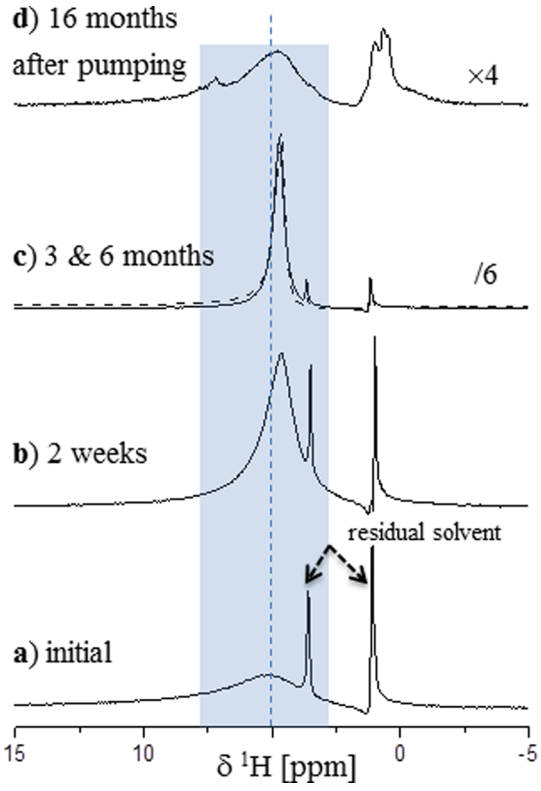

Figure 4. 300 MHz ^{1}H MAS NMR spectra of high-P ACC(*i*) as a function of time. The equal intensity of the mobile clustered waters peak at 3 and 6 months indicates they have reached their final state after ≤3 months. The 16 months spectrum, obtained after evacuation of the sample, shows the removal of the nonstructural, mobile waters.

shifts with time. The initial broad peak represents structural water molecules with reduced mobility that are homogeneously dispersed throughout the $ACC/PO_4^{3-}/H_2O$ solid.[49,50] With time, these water molecules are extracted from the phase separated calcite/HAp crystalline composite into clusters with increased mobility, attested by their gradual peak narrowing. The disappearance of this narrow peak after mild evacuation (10^{-2} Torr, 10 min) further supports the conclusion that it represents clusters of mobile water molecules. The weak and broad water peak is attributed to the remaining structural waters within the residual ACCP (Figure 4d). Our measurements clearly show that when vaterite and calcite have formed (e.g., after 2 weeks, Figure 4b), water clusters with increased mobility are detectable, however no HAp is yet detectable. This implies a slower crystallization of HAp and cHAp relative to calcite (or vaterite). The water molecules that are removed to intercrystalline regions are likely to assist or even enhance the diffusion and accumulation of calcium and phosphate. The overall process of HAp crystallization clearly occurs over a much longer time scale than the calcium carbonate crystallization.

All the above NMR spectra characterize the extraction of the water and phosphates from the carbonate rich phases that are driven by the transformation. However, thorough identification of the emerging *minor* components of the composite is possible only by also considering the {^{1}H,^{13}C} and {^{1}H,^{31}P} 2D-HETCOR spectra (Figure 5). These spectra show a set of

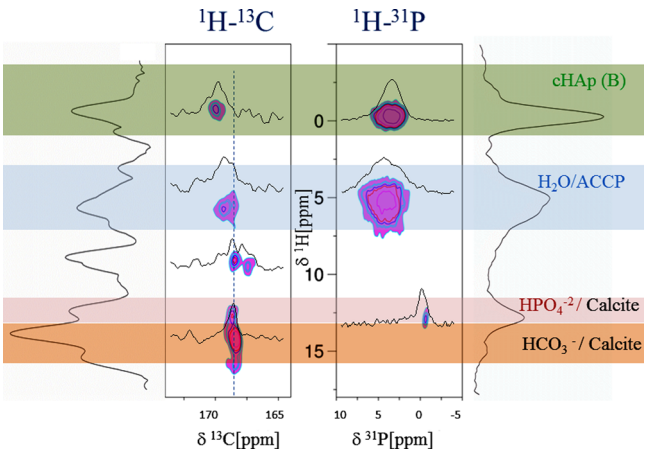

Figure 5. ^{1}H—^{13}C (left) and ^{1}H—^{31}P (right) 2D-HETCOR spectra of the high-P-ACC(*i*) after 16 months. The two respective spectral projections of the ^{1}H dimension are drawn vertically and annotated by peak assignments (on the right). The cross section projections along the ^{13}C and ^{31}P dimensions are obtained for each species (slab projections) and are drawn above each crosspeak. Assignments emerging from the HETCOR spectra are listed in Table 1.

{^{1}H,^{31}P} and {^{1}H,^{13}C} crosspeaks that establish connectivities within and across the carbonate- and phosphate-rich phases, and so refine the characterization of the interactions between them. The {^{1}H,^{31}P} and {^{1}H,^{13}C} 2D-HETCOR spectra are analyzed in parallel from the lowest to highest chemical shift of hydrogens.

The {^{1}H,^{31}P} spectrum exposes the characteristic hydroxyl-phosphate crosspeak {−0.2,3.3} of the HAp phase. This relatively narrow crosspeak indicates the presence of crystalline HAp in the emerging composite. The corresponding {^{1}H,^{13}C} crosspeak, {−0.8,170.6}, depicts hydrogens of similar hydroxyl character, and carbonates with B-type cHAp chemical shift, indicating that the respective carbonates are in molecular contact with the HAp phase. The reduced chemical shift value of this OH^- hydrogen implies that it is engaged in a strong hydrogen bond.[51]

The second and most pronounced set of crosspeaks (interactions) in the {^{1}H,^{13}C}, {^{1}H,^{31}P} 2D-HETCOR and the 2D-TEDOR spectra exposes the ^{31}P···^{1}H···^{13}C connectivity of the remaining structural water molecules with broad phosphate and carbonate peaks, representing the residual amorphous form of ACCP {169.2···3.9···5.5}. As noted above, these represent ACCP with higher structural uniformity than the initially precipitated phase.

Two crosspeaks within the {^{1}H,^{13}C} 2D-HETCOR show two carbonate-hydrogen pairs, {9.0,168.5} and {9.0,167.4}, representing carbonate species in carbon-rich phases. The fact that both carbonates, of which one is calcite, share common acidic hydrogens (9.0 ppm) suggests that the {9.0,167.4} crosspeak represents a defect within calcite.

DOI: 10.1021/ja511869g
J. Am. Chem. Soc. 2015, 137, 990−998

The HPO_4^{2-} species seen in the $\{^1H,^{31}P\}$ 2D-HETCOR spectrum {13.0,−0.6} shows cross-connectivity through this acidic hydrogen with calcite carbonates {13.0,168.5} in the $\{^1H,^{13}C\}$ 2D-HETCOR. Complemented by the well resolved $\{^{31}P,^{13}C\}$ 2D-TEDOR crosspeak, this $^{31}P\cdots^1H\cdots^{13}C$ connectivity represents calcite-entrapped intracrystalline HPO_4^{2-} structural defects. Last, the bicarbonate {14.3,168.5} crosspeak seen in the $\{^1H,^{13}C\}$ 2D-HETCOR spectrum (with no crossover peak to P) is indicative of intracrystalline bicarbonate defects entrapped in calcite. Such high ppm values of ^1H chemical shifts were observed in mollusk shells[39,52−54] and were occasionally named hydrogen carbonates[51] to distinguish them from bicarbonates with $\delta(^1H)$ as low as ∼7 ppm.

Stabilized Coprecipitate. When the high-P-ACC(*ii*) coprecipitate is first dehydrated at 50 °C for 2 days, it loses about 70% of its water content (SI Figure S3) and gives rise to an "indefinitely-stabilized" (over one year) amorphous form. In spite of the significant difference in the water/Ca mole ratio between the hydrated high-P-ACC(*i*) and the dehydrated high-P-ACC(*ii*), ∼1.6:1 vs ∼0.5:1, both initial coprecipitates appear as structurally indistinguishable homogeneous dispersions of phosphate and structural water molecules in ACC (SI Figure S7). The stabilization of the lower water content coprecipitate represents a locked metastable ACCP matrix, as that noted for stable biogenic ACC.

Transformation of the Low-P-ACC Hydrated and Dehydrated Coprecipitates. The low-P coprecipitate starts from a homogeneous dispersion of phosphates (3%, Figure 2b) and water molecules in ACC (ACCP) (SI Figures S4 and S8). This low-P-ACC undergoes a spontaneous phase separation and crystallization as the hydrated high-P-ACC(*i*). Spontaneous transformation occurs for both hydrated(*i*) and dehydrated(*ii*) samples, ∼1.25:1 and ∼0.4:1 water/Ca ratios. At the completion of the transformation, the resulting composite has the same structural characteristics as the transformed hydrated high-P ACC, albeit with lower abundances of ACCP, cHAp and HPO_4^{2-}, consistent with the lower P-content (SI Figure S5, Table 1). Since the low-P-ACC coprecipitates were monitored at the start and then after four months, whether an intermediate vaterite phase had formed could not be determined. In conclusion, the spontaneous transformation of the low hydration state seen here further emphasizes the combined role of phosphate and water. In the absence of high enough phosphate levels, the ACCP matrix is unstable, and spontaneously transforms into the crystalline phases.

■ DISCUSSION

Here we investigate ACC formed in the presence of phosphate (ACCP) using solid state NMR to characterize the materials in their initial state and to monitor their spontaneous transformation from the disordered ACCP phase into crystalline minerals. We also identify and characterize a kinetically locked ACCP phase arising under conditions of low hydration and high phosphate. We show that all initial ACCP phases are uniform molecular dispersions of phosphate and water in ACC ($ACC/PO_4^{3-}/H_2O$), where the chemical moieties appear to be identical regardless of the initial phosphate/water content. As phase separation and transformation into crystalline phases progress, calcite forms prevalently, whereas vaterite appears as a transient phase.[55] As time progresses, the initial ACCP never completely disappears, and an additional phase composed of cHAp and HAp also forms.

Solid state NMR reveals the molecular structures and interactions within the starting precipitates and during the transformation process that we discuss below. The REDOR model of the initial ACCPs reports that the phosphate dispersed in both high- and low-P ACCP phases is substantially lower than the total measured value. From this, we conclude that there are additional P-rich ACP-like phases in the initial material that are immiscible with the ACCP phase, possibly in the form of nanoscale islands of ACP. A similar observation was made in the gastroliths of *Cherax quadricarinatus*.[44,56,57]

The hydrated high-P-ACC(*i*), as well as both hydrated and "dehydrated" (about a third of the "hydrated" water content) low-P-ACC(*i*) and (*ii*), consist of a transient, spontaneously transforming ACCP phase, which yields calcite upon transformation, as well as HAp and cHAp as crystalline products, and residual ACCP. In addition, structural defects of bicarbonate and HPO_4^{2-} are entrapped in the calcite phase.

In the spontaneously transforming ACCP, after crystallization ensues, the residual ACCP phase (9 and 23% for low- and high-P-ACC, respectively) is structurally more homogeneous and more ordered than the starting phase, and possibly more tightly packed. Had this spontaneous process occurred entirely via a dissolution-recrystallization process, the initial solid solution of phosphate and water in calcium carbonate would have completely disappeared upon completion of the transformation. The persistence of a residual ACCP phase therefore implies that the process occurs at least in part by solid−solid phase transformation through phosphate ions and water extraction, rather than dissolution−recrystallization. This solid−solid transformation is hypothesized as one where, simultaneous with P/H_2O exclusion, calcium and carbonate ions are relocated to their positions at the respective lattice sites in a self-propagating manner.

Water is a key component in the transformation from the disordered phases to the ordered crystalline phases.[58] The change of the water chemical/structural environments along the transformation pathway is clearly visualized using solid state NMR. At the outset in the initial amorphous precipitate, the water molecules have restricted mobility and are identified as a structural component of the disordered phase of ACCP.[49] Thereafter, the water molecules are extracted from the crystallizing calcium carbonate matrix and form clusters with increased molecular mobility, possibly in between crystallites and/or at their surfaces. Some structural water molecules remain within the residual stabilized ACCP fraction, while other water molecules part to form the hydroxyls of HAp/cHAp, and the acidic hydrogens of the HPO_4^{2-} and HCO_3^- intracrystalline structural defects within calcite.

Observation of the products of crystallization in the NMR samples at the end of the process (after more than one year) shows faceted calcite crystals side-by-side with abundant nanoparticles (SI Figures S9 and S10). It is therefore plausible that water molecules which were released from the ACCP and accumulated may have led, at least partially, to recrystallization. These water molecules must have originated from the initial ACCP, because the samples were sealed during the whole transformation period. The observation of nanoparticles fusing to the crystals may be a testimony of a concomitant particle accretion process,[24] however, when the recrystallization occurred is not known.

The very late formation of the minor crystalline phases of HAp/cHAp occurs when calcite is abundant. This therefore indicates that the faster process of calcite buildup is the

DOI: 10.1021/ja511869g
J. Am. Chem. Soc. 2015, 137, 990−998

dominant driving force of the overall transformation. It is implied that the structural water molecules released during calcite crystallization facilitate and enhance the surface diffusion of the phosphate anions (and of calcium counterions), until sufficiently large numbers accumulate and crystallize into HAp/cHAp.

The fact that unlike ACCP, the control hydrated ACP precipitate does not show similar spontaneous crystallization indicates that neither water molecules, nor phosphates can diffuse within ACP. This difference further substantiates the notion that it is the combination of gradual extraction of water molecules and phosphate anions from the ACCP matrix which enables/drives the subsequent cHAp/HAp crystallization. This slower transformation must take place within an H_2O-rich environment (water clusters to be distinguished from bulk water), implying that it proceeds through an ion-by-ion precipitation process. In this water-assisted process, water has the essential role of facilitating the transport—ion diffusion and aggregation of Ca^{2+}, phosphates, and carbonates, and the source of hydroxyls for HAP/cHAP buildup.

The locked state of the high-P-ACC(*ii*) phase was achieved by rapid extraction of the initial water (48 h at 50 °C), during which phosphate migration did not occur. This observation suggests that during this mild heating, phosphate migration is slower than water extraction. This in turn leads to the conclusion that for the spontaneous crystallization process to take place, phosphate and water extraction must occur in concert since below sufficient water levels, locking of the phosphate within the ACCP phase occurs. For the low-P-ACC, stabilization of the amorphous phase does not occur, regardless of the initial water level, indicating that the level of phosphates is too low to stabilize the system and inhibit crystallization.

The stabilization observed for dehydrated high-P-ACC(*ii*), (~0.5:1 water/Ca ratio) may either reflect the fact that the system is kinetically locked, or alternatively that the resulting precipitate is thermodynamically (more) stable. Combined with the evidence of the heat-induced transformations (SI Figure S2), we conclude that the observed stabilization is primarily due to geometric frustration that locks the system in a thermodynamically metastable state. This stabilization relies on the combination of two factors, P- and H_2O-content: in the absence of sufficient water, yet when the phosphate level is high enough, the latter becomes locked within ACC, thus preventing crystallization.

Our in vitro experiments with transient and stable ACC parallel biogenic ACC pathways, where the hydration levels within ACC are controlled by organisms as a means of regulating the fate of the biomineral either as a stable phase or as a transient phase.[59] ACC formed in biology usually contains additives that enable its formation in the first place, and determine whether the ACC will be transient or stable.[17,37,60] Phosphate is a commonly used additive in biology for ACC production, particularly among the crustaceans,[34] but also in ascidians.[61] The mineral of the lobster carapace, for example, was described as being composed of a mixture of stable ACC and ACP, however, in the absence of characterization means, whether molecular dispersions occur remained an open question.[35] Interestingly, a later study of the lobster carapace showed how two crystalline phases—calcite and carbonated hydroxyapatite—were formed by heating the initial disordered mineral, and led to the hypothesis that the starting amorphous material is a molecular dispersion of phosphate in ACC.[34] Our NMR distinctions for the synthetic homogeneous ACCP dispersions studied here, heated (SI) or spontaneously transforming at ambient conditions, clearly involve phase separation and crystallization and result in the same crystalline products as those of the heated biogenic carapace. This similarity supports the hypothesis that the lobster carapace consists of ACCP, like that observed in its gastroliths, and further emphasizes the relevance of the insight gained from the in vitro processes observed here to biogenic ones.

■ CONCLUSIONS

Upon coprecipitation, phosphate and water form metastable homogeneous dispersions in amorphous calcium carbonate. Depending on the initial molar ratio of these two additives, the resulting precipitates may spontaneously transform to the crystalline products—calcite and cHAp/HAp, or retain indefinitely their metastable, disordered locked form. The spontaneous process is driven by the thermodynamically favored calcite crystallization. It proceeds via phase separation with water and phosphate simultaneously diffusing out of the disordered mixed phase, enabling first solid—solid phase transformation and crystallization of calcite, concomitant with partial formation of a vaterite intermediate. The extracted P and H_2O clusters induce the subsequent crystallization of HAp/cHAp via a classical water-mediated[62] precipitation process. In the locked disordered phase, in the absence of sufficiently high water content, the high P-content can no longer diffuse and phase separate, hence, geometric hindrance counteracts the thermodynamic driving forces.

The spontaneously transforming and the locked ACC forms mirror the transient and stable ACC biomineralization pathways, respectively. This study thus highlights the importance of water and small ionic additives, such as phosphates in biomineralization processes. The fundamental molecular level factors unraveled in this study primarily by solid state NMR bear immediate relevance to bioinspired rational design of functional materials.

■ EXPERIMENTAL SECTION

Precipitation Procedure. Three ACC samples with different phosphate concentrations were prepared. In the synthesis reaction, **1** mL of 100 mM calcium chloride solution was used as the calcium source. For the phosphate-free sample, 1 mL of 100 mM sodium carbonate solution was the carbonate source. For the low-phosphate ACC sample, 1 mL solution containing 92.5 mM sodium carbonate and 6 mM sodium phosphate solution was used as carbonate and phosphate source. One ml solution containing 77.5 mM sodium carbonate and 18 mM sodium phosphate solution was used as carbonate and phosphate source to prepare the high-phosphate ACC (All reagents by Sigma). The carbonate and phosphate concentrations were chosen to provide similar anionic equivalent concentrations in the reaction based on the assumption that carbonate precipitate with calcium on a 1:1 ratio and phosphate precipitate with calcium on a 1:1.33 ratio. The carbonate stock solution was buffered by adding NaOH solution to the same pH of the phosphate solution (pH = 12.4) so all carbonate and phosphate solutions have the same pH. The solutions were cooled to 0°–4 °C. The carbonate and phosphate solution was added to the calcium chloride solution to yield a 2 mL reaction volume. Immediately after mixing, the solution was filtered with a Durapore membrane filter (Merck), washed with absolute ethanol, and dried under an IR lamp. The dried precipitates were kept in an argon environment at ambient temperature. The samples used for NMR analysis were enriched to 15% ^{13}C by diluting 98% ^{13}C solution with unenriched stock. Two sets of samples were prepared: (*i*) hydrated, as-prepared after 30 min under an IR lamp; (*ii*)

DOI: 10.1021/ja511869g
J. Am. Chem. Soc. 2015, 137, 990–998

dehydrated, after 50 °C for 2 days prior to NMR measurements, as indicated in the main text.

Solid State NMR. 75.69 MHz ^{13}C, 121.85 MHz ^{31}P, 300.01 MHz ^{1}H solid state MAS NMR measurements were carried out on a triple-channel, solid state AVANCE III NMR spectrometer (Bruker), equipped with triple-resonance probe with a 4 mm spinning module. Samples, ∼40 mg, were packed in 4 mm (o.d.) zirconia rotors; rotors were kept closed and maintained constant weight (no weight loss). The experimental schemes employed excitation ($\pi/2$) and refocusing (π) pulses of 5.0 and 10.0 μs widths, an echo interval, τ, identical to the rotor period, T_R, ^{1}H SPINAL decoupling at a level of 100 kHz, Hartmann−Hahn rf levels at 50 kHz for ^{13}C and ^{31}P, and 1H ramped CP (70−100 kHz). Other experimental and acquisition parameters are summarized in SI Table S3.

^{13}C{^{31}P} and ^{31}P{^{13}C } REDOR experiments were conducted using a REDOR pulse sequence with refocusing π pulses after each rotor period (T_R) on the observed channel and dephasing π pulses at the middle of each rotor period on the nonobserved nucleus, followed by an additional $2T_R$ period with a π-pulse in the middle to simultaneously form Hahn- and rotational echos. REDOR π pulses employed xy-8 phase cycling for the refocusing and recoupling pulses.[42,43,63] Data acquisition employed an alternating block scheme, collecting a single S_0 transient with recoupling pulses turned off, followed by S_R transient collection with recoupling pulses turned on. Each part was processed to yield the respective spectrum. REDOR difference spectra, ΔS, obtained via $S_0 - S_R$ subtraction, exclusively exhibit peaks of dipolar-coupled chemical species. The REDOR data presented in the manuscript were collected using the CP and DE excitation schemes.

The 2D-TEDOR ^{31}P···^{13}C experiment was run employing $8 \times 8T_R$ TEDOR mixing.[64] This experiment starts with ^{1}H→^{31}P CP followed by a t_1 evolution period, which encodes the isotropic chemical shift of the ^{31}P ($\Delta t_1 = T_R$). The subsequent TEDOR mixing is made up of $8T_R$ REDOR dipolar recoupling blocks in the preparation and buildup periods, i.e., before and after the (central) coherence transfer step via the two back-to-back $\pi/2$-pulses (on the ^{31}P- and ^{13}C- nuclei). During TEDOR preparation the refocusing π-pulses are on the ^{31}P-channel (recoupling pulses in the middle of each rotor period on the ^{13}C channel), and during the buildup period, they are on the ^{13}C-channel (recoupling pulses on the ^{31}P). Similar to the REDOR sequence above, an additional $2T_R$ period with a π-pulse in the middle is added to form simultaneously a Hahn and a rotational echo.

^{1}H{^{31}P/^{13}C} 2D-HETCOR experiments were run employing the wPMLG5[65] homonuclear decoupling scheme during t_1 for the ^{1}H chemical shift evolution period. ^{1}H{^{13}C} 2D-HETCOR of glycine was optimized first for ^{1}H resolution and also served to calibrate the ^{1}H chemical shift scale. Time-proportional phase incrementation (TPPI)[29] was used to obtain purely absorptive 2D NMR spectra with frequency sign discrimination along the indirect dimension. The chemical shifts of ^{13}C, ^{31}P, and ^{1}H are reported relative to TMS, 85% H_3PO_4 and adamantane, respectively, within ±0.1 ppm. REDOR simulations were performed using Simpson.[66] Peak areas were calculated by deconvolution using DMFIT[67] and Topspin.

■ ASSOCIATED CONTENT

Supporting Information

Table S1: element composition and water content in coprecipitates; Table S2: ^{13}C{^{31}P} REDOR $\Delta S/S_0$ values of components in initial and final coprecipitates; Table S3: experimental NMR parameters; Figure S1: electron microscope images; Figure S2: FTIR spectra; Figure S3: TGA analysis; Figure S4: ^{13}C, ^{31}P CP/DE-MAS and ^{1}H NMR spectra; Figure S5: 2D spectra of low-P-ACC; Figure S6: ^{13}C{^{31}P} DE- and CP-REDOR; Figure S7: ^{1}H, ^{31}P (CP), ^{13}C (CP and DE) MAS NMR spectra of the stable high-P-ACC coprecipitate; Figure S8: ^{13}C{^{31}P} DE- and CP-REDOR MAS NMR spectra of low-P-ACC; and Figures S9, S10: SEM micrographs. This material is available free of charge via the Internet at http://pubs.acs.org.

■ AUTHOR INFORMATION

Corresponding Authors

chrschm@tx.technion.ac.il.
Assaf.Gal@mpikg.mpg.de.

Present Address

[§]Department of Biomaterials, Max-Planck Institute of Colloids and Interfaces, Potsdam, Germany.

Author Contributions

The manuscript was written through contributions of all authors.

Notes

The authors declare no competing financial interest.

■ ACKNOWLEDGMENTS

The authors thank Prof. Peter Fratzl and Dr. Wouter Habraken from the Max Plank Institute for Colloids and Interfaces, Potsdam-Golm for useful discussions and exchange of information; May Bokobza and Ekaterina Zaslavski from the Technion for assistance with data handling and graphics. This research was supported by Israel Science Foundation Grant 1345/11, by RBNI Nevet Grant 03-2010, and by a German Research Foundation grant within the framework of the Deutsch−Israelische Projektkooperation. L.A. is the incumbent of the Dorothy and Patrick Gorman Professorial Chair of Biological Ultrastructure, and S.W. of the Dr. Trude Burchardt Professorial Chair of Structural Biology.

■ REFERENCES

(1) Simkiss, K.; Wilbur, K. M. *Biomineralization*; Academic Press: San Diego, CA, 1989;, pp 337.
(2) Lowenstam, H. A. *Science* **1981**, *211*, 1126−1131.
(3) Lowenstam, H. A.; Weiner, S. *On Biomineralization*; Oxford University Press: New York, 1989; pp 324.
(4) Nudelman, F.; Sommerdijk, N. A. J. M. *Angew. Chem., Int. Ed. Engl.* **2012**, *51*, 6582−6596.
(5) Weiner, S.; Addadi, L. *Annu. Rev. Mater. Res.* **2011**, *41*, 21−40.
(6) Meldrum, F. C.; Coelfen, H. *Chem. Rev.* **2008**, *108*, 4332−4432.
(7) Vidavsky, N.; Addadi, S.; Mahamid, J.; Shimoni, E.; Ben-Ezra, D.; Shpigel, M.; Weiner, S.; Addadi, L. *Proc. Natl. Acad. Sci. U. S. A.* **2014**, *111*, 39−44.
(8) Beniash, E.; Addadi, L.; Weiner, S. *J. Struct. Biol.* **1999**, *125*, 50−62.
(9) Killian, C. E.; Wilt, F. H. *Chem. Rev.* **2008**, *108*, 4463−4474.
(10) Wilt, F. H. *Dev. Biol.* **2005**, *280*, 15−25.
(11) Koga, N.; Nakagoe, Y. Z.; Tanaka, H. *Thermochim. Acta* **1998**, *318*, 239−244.
(12) Brecevic, L.; Nielsen, A. E. *J. Cryst. Growth* **1989**, *98*, 504−510.
(13) Loste, E.; Wilson, R. M.; Seshadri, R.; Meldrum, F. C. *J. Cryst. Growth* **2003**, *254*, 206−218.
(14) Gal, a.; Weiner, S.; Addadi, L. *J. Am. Chem. Soc.* **2010**, *132*, 13208−13211.
(15) Dillaman, R.; Hequembourg, S.; Gay, M. *J. Morphol.* **2005**, *263*, 356−374.
(16) Kellermeier, M.; Melero-Garcia, E.; Glaab, F.; Klein, R.; Drechsler, M.; Rachel, R.; Manuel Garcia-Ruiz, J.; Kunz, W. *J. Am. Chem. Soc.* **2010**, *132*, 17859−17866.
(17) Wang, D.; Wallace, A. F.; De Yoreo, J. J.; Dove, P. M. *Proc. Natl. Acad. Sci. U. S. A.* **2009**, *106*, 21511−21516.
(18) De Yoreo, J. J.; Vekilov, P. G. *Biomineralization* **2003**, *54*, 57−93.
(19) Ramirez, A. P. *Nature* **2003**, *421*, 483.
(20) Raz, S.; Hamilton, P. C.; Wilt, F. H.; Weiner, S.; Addadi, L. *Adv. Funct. Mater.* **2003**, *13*, 480−486.

DOI: 10.1021/ja511869g
J. Am. Chem. Soc. 2015, 137, 990−998

(21) Sato, A.; Nagasaka, S.; Furihata, K.; Nagata, S.; Arai, I.; Saruwatari, K.; Kogure, T.; Sakuda, S.; Nagasawa, H. *Nat. Chem. Biol.* **2011**, *7*, 197−199.
(22) Akiva-Tal, A.; Kababya, S.; Balazs, Y. S.; Glazer, L.; Berman, A.; Sagi, A.; Schmidt, A. *Proc. Natl. Acad. Sci. U. S. A.* **2011**, *108*, 14763−14768.
(23) Gower, L. B. *Chem. Rev.* **2008**, *108*, 4551−4627.
(24) Gal, A.; Kahil, K.; Vidavsky, N.; DeVol, R. T.; Gilbert, P. U. P. A.; Fratzl, P.; Weiner, S.; Addadi, L. *Adv. Funct. Mater.* **2014**, *24*, 5420−5426.
(25) Shechter, A.; Glazer, L.; Cheled, S.; Mor, E.; Weil, S.; Berman, A.; Bentov, S.; Aflalo, E. D.; Khalaila, I.; Sagi, A. *Proc. Natl. Acad. Sci. U. S. A.* **2008**, *105*, 7129−7134.
(26) Lowenstam, H. A.; Weiner, S. *Science* **1985**, *227*, 51−53.
(27) Yang, L.; Killian, C. E.; Kunz, M.; Tamura, N.; Gilbert, P. U. P. A. *Nanoscale* **2011**, *3*, 603−609.
(28) Dauphin, Y. *Palaeont. Z.* **2001**, *75*, 113−122.
(29) Sethmann, I.; Hinrichs, R.; Worheide, G.; Putnis, A. *J. Inorg. Biochem.* **2006**, *100*, 88−96.
(30) Cuif, J.; Dauphin, Y. *J. Struct. Biol.* **2005**, *150*, 319−331.
(31) Sethmann, I.; Putnis, A.; Grassmann, O.; Löbmann, P. *Am. Mineral.* **2005**, *90*, 1213−1217.
(32) Politi, Y.; Metzler, R. A.; Abrecht, M.; Gilbert, B.; Wilt, F. H.; Sagi, I.; Addadi, L.; Weiner, S.; Gilbert, P. U. P. A. *Proc. Natl. Acad. Sci. U. S. A.* **2008**, *105*, 20045−20045.
(33) Perez-Huerta, A.; Dauphin, Y.; Cusack, M. *Micron* **2013**, *44*, 395−403.
(34) Al-Sawalmih, A.; Li, C. H.; Siegel, S.; Fratzl, P.; Paris, O. *Adv. Mater.* **2009**, *21*, 4011−4015.
(35) Becker, A.; Ziegler, A.; Epple, M. *Dalton Trans.* **2005**, 1814−1820.
(36) Levi-Kalisman, Y.; Raz, S.; Weiner, S.; Addadi, L.; Sagi, I. *Adv. Funct. Mater.* **2002**, *12*, 43−48.
(37) Gong, Y. U. T.; Killian, C. E.; Olson, I. C.; Appathurai, N. P.; Amasino, A. L.; Martin, M. C.; Holt, L. J.; Wilt, F. H.; Gilbert, P. U. P. A. *Proc. Natl. Acad. Sci. U. S. A.* **2012**, *109*, 6088−6093.
(38) Nielsen, M. H.; Aloni, S.; De Yoreo, J. J. *Science* **2014**, *345*, 1158−1162.
(39) Ben Shir, I.; Kababya, S.; Katz, I.; Pokroy, B.; Schmidt, A. *Chem. Mater.* **2013**, *25*, 4595−4602.
(40) Ben Shir, I.; Kababya, S.; Schmidt, A. *Isr. J. Chem.* **2014**, *54*, 74−85.
(41) Veshtort, M.; Griffin, R. G. *J. Magn. Reson.* **2006**, *178*, 248−282.
(42) Gullion, T.; Schaefer, J. *J. Magn. Reson.* **1989**, *81*, 196−200.
(43) Gullion, T.; Schaefer, J. *Adv. Magn. Reson.* **1989**, *13*, 57−83.
(44) Gertman, R.; Ben Shir, I.; Kababya, S.; Schmidt, A. *J. Am. Chem. Soc.* **2008**, *130*, 13425−13432.
(45) Babonneau, F.; Bonhomme, C.; Hayakawa, S.; Osaka, A. *Mater. Res. Soc. Symp. Proc.* **2007**, *984*, 39.
(46) Beshah, K.; Rey, C.; Glimcher, M. J.; Schimizu, M.; Griffin, R. G. *J. Solid State Chem.* **1990**, *84*, 71−81.
(47) Jäger, C.; Welzel, T.; Meyer-Zaika, W.; Epple, M. *Magn. Reson. Chem.* **2006**, *44*, 573−580.
(48) Vyalikh, A.; Simon, P.; Kollmann, T.; Kniep, R.; Scheler, U. *J. Phys. Chem. C* **2011**, *115*, 1513−1519.
(49) Ihli, J.; Wong, W. C.; Noel, E. H.; Kim, Y. Y.; Kulak, A. N.; Christenson, H. K.; Duar, M. j.; Meldrum, F. C. *Nat. Commun.* **2013**, *5*, 3169.
(50) Schmidt, M. P.; Ilott, A. J.; Phillips, B. L.; Reeder, R. J. *Cryst. Growth Des.* **2014**, *14*, 938−951.
(51) Tsai, T. W. T.; Chan, J. C. C. *ANN. R. NMR S.* **2011**, *73*, 1−61.
(52) Feng, J.; Lee, Y. J.; Reeder, R. J.; Phillips, B. L. *Am. Mineral.* **2006**, *91*, 957−960.
(53) Jager, C.; Colfen, H. *CrystEngComm* **2007**, *9*, 1237−1244.
(54) Phillips, B. L.; Lee, Y. J.; Reeder, R. J. *Environ. Sci. Technol.* **2005**, *39*, 4533−4539.
(55) Hasse, B.; Ehrenberg, H.; Marxen, J. C.; Becker, W.; Epple, M. *Chem.—Eur. J.* **2000**, *6*, 3679−3685.
(56) Bentov, S.; Weil, S.; Glazer, L.; Sagi, A.; Berman, A. *J. Struct. Biol.* **2010**, *171*, 207−215.
(57) Raz, S.; Testeniere, O.; Hecker, A.; Weiner, S.; Luquet, G. *Biol. Bull.* **2002**, *203*, 269−274.
(58) Raiteri, P.; Gale, J. D. *J. Am. Chem. Soc.* **2010**, *132*, 17623−17634.
(59) Dorvee, J. R.; Veis, A. *J. Struct. Biol.* **2013**, *183*, 278−303.
(60) Politi, Y.; Mahamid, J.; Goldberg, H.; Weiner, S.; Addadi, L. *CrystEngComm* **2007**, *9*, 1171−1177.
(61) Levi-Kalisman, Y.; Raz, S.; Weiner, S.; Addadi, L.; Sagi, I. *J. Chem. Soc., Dalton Trans.* **2000**, 3977−3982.
(62) Hasse, B.; Ehrenberg, H.; Marxen, J. C.; Becker, W.; Epple, M. *Chem.—Eur. J.* **2000**, *6*, 3679−3685.
(63) Gullion, T.; Baker, D. B.; Conradi, M. S. *J. Magn. Reson.* **1990**, *89*, 479−484.
(64) Hing, A. W.; Vega, S.; Schaefer, J. *J. Magn. Reson.* **1992**, *96*, 205−209.
(65) Leskes, M.; Vega, S. *J. Chem. Phys.* **2009**, *130*, 124506−124512.
(66) Bak, M.; Rasmussen, J. T.; Nielsen, N. C. *J. Magn. Reson.* **2000**, *147*, 296−330.
(67) Massiot, D.; Fayon, F.; Capron, M.; King, I.; Calvé, S. L.; Alonso, B.; Durand, J.; Bujoli, B.; Gan, Z.; Hoatson, G. *Magn. Reson. Chem.* **2002**, *40*, 70−76.

DOI: 10.1021/ja511869g
J. Am. Chem. Soc. 2015, 137, 990−998